

Anticyclonic Eddy Sheddings from Kuroshio Loop and the Accompanying Cyclonic Eddy in the Northeastern South China Sea

ZHIWEI ZHANG AND WEI ZHAO

Physical Oceanography Laboratory/CIMST, Ocean University of China, and Qingdao National Laboratory for Marine Science and Technology, Qingdao, China

BO QIU

Department of Oceanography, University of Hawai'i at Mānoa, Honolulu, Hawaii

JIWEI TIAN

Physical Oceanography Laboratory/CIMST, Ocean University of China, and Qingdao National Laboratory for Marine Science and Technology, Qingdao, China

(Manuscript received 7 August 2016, in final form 9 March 2017)

ABSTRACT

Sheddings of Kuroshio Loop Current (KLC) eddies in the northeastern South China Sea (SCS) are investigated using mooring arrays, multiple satellite data, and data-assimilative HYCOM products. Based on altimeter sea surface heights between 1992 and 2014, a total of 19 prominent KLC eddy shedding (KLCES) events were identified, among which four events were confirmed by the concurrent moored and satellite observations. Compared to the leaping behavior of Kuroshio, KLCES is a relatively short-duration phenomenon that primarily occurs in boreal autumn and winter. The KLC and its shedding anticyclonic eddy (AE) trap a large amount of Pacific water with high temperature–salinity and low chlorophyll concentration in the upper layer. The corresponding annual-mean transport caused by KLCES reaches 0.24–0.38 Sv (1 Sv = $10^6 \text{ m}^3 \text{ s}^{-1}$), accounting for 6.8%–10.8% of the upper-layer Luzon Strait transport. Altimeter-based statistics show that among ~90% of the historical KLCES events, a cyclonic eddy (CE) is immediately generated behind the AE southwest of Taiwan. Both energetics and stability analyses reveal that because of its large horizontal velocity shear southwest of Taiwan, the northern branch of KLC is strongly unstable and the barotropic instability of KLC constitutes the primary generation mechanism for the CE. After CE is generated, it quickly grows and gradually migrates southward, which in turn facilitates the detachment of AE from KLC. The intrinsic relationship between KLC and CE explains well why eddy pairs are commonly observed in the region southwest of Taiwan.

1. Introduction

The South China Sea (SCS) is the largest and semi-enclosed marginal sea in the western Pacific, which directly connects with the Pacific Ocean through the

Luzon Strait (Fig. 1). Research of past decades indicates that SCS is abundant with multiscale dynamical processes, including wind-driven and thermohaline circulation (Qu 2000; Su 2004; Wang et al. 2011), energetic mesoscale eddies (Wang et al. 2003; Zhang et al. 2013), strong internal waves (Alford et al. 2015; Huang et al. 2016), and enhanced turbulent mixing (Tian et al. 2009; Yang et al. 2016). Among these processes, mesoscale eddies with spatial–temporal scales of 50–300 km and 10–100 days and strong kinetic energies are observed to be crucial in connecting the large- and small-scale processes (Zhang et al. 2016). In addition, mesoscale eddies have been found to play important roles in transporting oceanic materials (nonnegligible compared to the

Denotes content that is immediately available upon publication as open access.

Supplemental information related to this paper is available at the Journals Online website: <http://dx.doi.org/10.1175/JPO-D-16-0185.1>.

Corresponding author: J. Tian, tianjw@ouc.edu.cn; Z. Zhang, zzw330@ouc.edu.cn

DOI: 10.1175/JPO-D-16-0185.1

© 2017 American Meteorological Society. For information regarding reuse of this content and general copyright information, consult the [AMS Copyright Policy](#) (www.ametsoc.org/PUBSReuseLicenses).

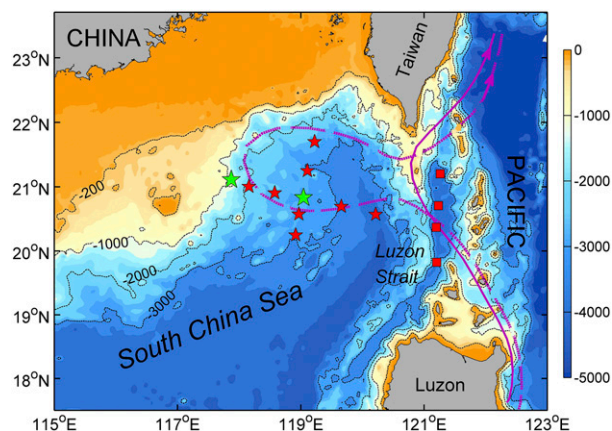


FIG. 1. Bathymetry (m) in the northeastern SCS and western Pacific. Green stars, red squares, and red stars indicate mooring locations during the periods of April 2011–April 2012, April 2012–April 2013, and October 2013–June 2014, respectively. The purple solid and dashed lines represent the leaping and looping paths of Kuroshio, respectively. The isobaths of 200, 1000, 2000, and 3000 m are indicated by black dashed lines.

large-scale circulation; Zhang et al. 2013), modulating basin-scale circulation (Yang and Liu 2003), and affecting small-scale internal waves in the SCS (Xie et al. 2015; Huang et al. 2017).

As verified by both satellite and in situ observations, the region west of Luzon Strait (i.e., the northeastern SCS) is one of the richest sources of mesoscale eddies within the SCS (D. Wang et al. 2008; Chen et al. 2011; Zhang et al. 2013, 2016; and references therein). Although other generation mechanisms were proposed (G. Wang et al. 2008; Zheng et al. 2011), a large number of these eddies are believed to shed from the Kuroshio loop or arise from variability of the Kuroshio path (Metzger and Hurlburt 2001; Jia and Chassignet 2011; Nan et al. 2011b; Sun et al. 2016). Because of their importance for the materials and energy budget of SCS, the Kuroshio loop and its associated eddy shedding have been repeatedly studied since the 1980s. By analyzing historical hydrographic data, Li and Wu (1989) first named the Kuroshio path in the northeastern SCS the Kuroshio Loop Current (KLC; see purple dashed line in Fig. 1) by analogy to the Loop Current in the Gulf of Mexico and proposed the possibility that eddies may shed from the KLC and intrude into SCS. The study of Li et al. (1998) claimed that they had directly observed an anticyclonic eddy (AE) originating from the Kuroshio (containing Kuroshio water) in September 1994. Some later studies, for example, Farris and Wimbush (1996), Metzger and Hurlburt (2001), Centurioni et al. (2004), Jia and Liu (2004), and Jia et al. (2005), generally accepted the idea of KLC and eddy shedding west of Luzon Strait. However, these investigations were based on either

numerical models or fragmentary observations and did not provide convincing proofs to demonstrate this phenomenon. Through the analyses of altimeter sea surface heights (SSHs) with improved mean dynamic topography (MDT) and satellite-tracked trajectories of surface drifters, recent statistical studies gave more evidence for the KLC and eddy shedding phenomena (Caruso et al. 2006; Jia and Chassignet 2011; Nan et al. 2011a; Guo et al. 2013). Importantly, these studies pointed out that the KLC and its associated eddy shedding are only a transient, rather than persistent, phenomenon that primarily occurs in the winter seasons in the northeastern SCS; for most of the time, the Kuroshio leaps across the Luzon Strait and directly connects to the east of Taiwan (see purple solid line in Fig. 1), which is quite different from the situation of the Loop Current in the Gulf of Mexico (Oey et al. 2005).

Regarding the abovementioned KLC and eddy shedding phenomena, however, there also exist different views. For example, the altimeter-based study of Yuan et al. (2006) argued that most of the so-called KLCs in winter were actually only anticyclonic intrusions of Kuroshio because there existed only westward but no eastward flows in the Luzon Strait during those cases. Their subsequent study (Yuan et al. 2007) further pointed out that the AE reported by Li et al. (1998) was actually generated to the northwest of the Luzon Island rather than shed from KLC. If an eddy was shed from the KLC, the majority of its water mass should come from the Kuroshio with high temperature–salinity (T – S) in the surface and subsurface layers (Qu et al. 2000). Therefore, it is difficult to judge whether an eddy is truly shed from the KLC solely based on satellite observations and sparse in situ data. To the authors' knowledge, only two cases of AE shedding from the KLC were ever reported with certainty until now based on concurrent satellite and in situ T – S observations (D. Wang et al. 2008; Zhang et al. 2016).

While these previous studies have improved our knowledge of KLC and the associated eddy sheddings, several important issues remain to be addressed. First, the detailed circulation pattern of the Kuroshio intrusion before the eddy shedding, in terms of Loop Current versus anticyclonic intrusion (i.e., only inflow or inflow–outflow currents in the Luzon Strait), is still debatable (Yuan et al. 2006; Jia and Chassignet 2011). Second, because of the lack of systematic in situ observations, water mass characteristics within the eddies from KLC are not fully understood, and the equivalent volume transport caused by the eddy sheddings is also unknown. Third, and most importantly, the mechanism of the eddy sheddings from the Kuroshio intrusion is not fully understood. By analyzing long-term altimeter data,

recent studies found that there is usually a cyclonic eddy (CE) generated to the northeast of AE after it was shed from the KLC (Nan et al. 2011b; Zhang et al. 2016). The extent to which such a CE contributes to the AE shedding and the exact generation mechanism of the CE, however, has not been clarified by these studies.

In this paper, the abovementioned issues regarding the KLC eddy shedding (KLCES) are examined through the synergetic use of moored and satellite-derived data and data-assimilative model products. The rest of this paper is organized as follows: Section 2 introduces the data and model products used in this study. Section 3 presents characteristics of KLCES revealed by the concurrent satellite and moored observations. In section 4, the mechanism of the eddy shedding is examined. Finally, the summary and discussion are given in section 5.

2. Data and model products

a. Moored data

To investigate the eddy shedding processes from the KLC and the three-dimensional structure of the associated eddies, extensive moored observations were conducted in the regions west of and inside the Luzon Strait from April 2011 to June 2014 (Fig. 1; Zhang et al. 2013, 2015, 2016). The entire moored observations consist of three segments and were carried out during April 2011–April 2012, April 2012–April 2013, and October 2013–June 2014, respectively. In the first and third segments, two and eight bottom-anchored subsurface moorings were deployed in the region west of the Luzon Strait, respectively, and in the second segment four similar moorings were deployed inside the Luzon Strait (Fig. 1). All the moorings were heavily equipped with acoustic Doppler current profilers (ADCPs), recording current meters, and T – S chains to measure current velocity and T – S over nearly the whole water column. Details of the instrumental configurations of the moorings can be found in Zhang et al. (2013, 2015, 2016). To study water mass characteristics of eddies shed from the KLC, moored T – S data in the region west of the Luzon Strait were used in this study. In addition, to depict the circulation pattern of Kuroshio in the Luzon Strait, the moored velocity data in the Luzon Strait were used.

b. Satellite data

To examine the surface characteristics of KLCES, satellite altimeter data of sea level anomaly (SLA) and SSH between October 1992 and October 2014 from the Archiving, Validation, and Interpretation of Satellite Oceanographic Data (AVISO; <http://www.aviso.oceanobs.com/>) were used in this study. Both the SLA and SSH data used

here are gridded datasets with spatial and temporal resolutions of $1/4^\circ$ and 1 day, respectively. This newly released SLA dataset merged observations from different altimetry satellites [TOPEX/Poseidon, Jason-1/2, Envisat, Geosat Follow-On (GFO), and ERS-1/2] and significantly improved tidal and atmospheric barometric corrections when compared with the old version (Volkov et al. 2007). The SSH here is the sum of SLA and a new version of MDT, which was produced by Rio et al. (2013) through the synergetic use of space gravity data, altimetry, and multiple in situ measurements. By taking into account the most recent geoid mean field and more in situ dataset, the new MDT has improved precision compared to its earlier version (Rio et al. 2009). Comparison between the surface currents obtained from drifters and MDT (through geostrophic calculation) reveals very close circulation patterns and velocity magnitudes inside and west of the Luzon Strait (see Fig. S1 in the supplementary materials), demonstrating the good quality of MDT in this specific region.

In addition to the AVISO altimeter data, sea surface temperature (SST) and near-surface concentration of chlorophyll (CHL) of the Moderate Resolution Imaging Spectroradiometer (MODIS) were obtained from NASA's OceanColor website (<http://oceancolor.gsfc.nasa.gov>). The MODIS-derived SST and CHL data used here are the level-3, 8-day composite products that have a spatial resolution of 4 km. Considering the bad data retrieval due to cloud covers, only two periods with good SST and CHL coverage (i.e., November 2011–February 2012 and November 2012–December 2012) were selected here to study the KLC and the associated eddies.

c. HYCOM products

The global $1/12^\circ$ reanalysis products of the Hybrid Coordinate Ocean Model (HYCOM) that adopts the Navy Coupled Ocean Data Assimilation were acquired from the HYCOM data server (<http://hycom.org/dataserver/glb-reanalysis>). This system has assimilated multiple observational data, including satellite altimeter, SST data, and in situ T – S profiles from different instruments (e.g., CTDs, XBTs, and Argo floats). The HYCOM products (including three-dimensional velocity and T – S fields) are archived every day and have 40 layers in vertical. Previous comparisons between the HYCOM products and in situ velocity and T – S data revealed that the HYCOM performed well in simulating eddies and Kuroshio intrusions in the northern SCS (Park and Farmer 2013; Zhang et al. 2013; Huang et al. 2016, 2017). The HYCOM velocity and T – S data between 2009 and 2013 are used in this study to investigate the generation mechanism of the CE southwest of Taiwan and its connection to the KLCES.

TABLE 1. Information of the prominent KLCES events between October 1992 and October 2014.

No.	Start date of KLC	Shedding date of AE	End date of AE	Demise location of AE	CE exists
1	2 Dec 1992	3 Feb 1993	19 May 1993	16.5°N, 112.0°E	Yes
2	2 Nov 1994	22 Feb 1995	31 May 1995	18.5°N, 113.0°E	Yes
3	23 Oct 1996	8 Jan 1997	7 May 1997	17.0°N, 112.5°E	Yes
4	24 Sep 1997	31 Dec 1997	11 Feb 1998	19.5°N, 114.5°E	Yes
5	24 Nov 1999	23 Feb 2000	26 Apr 2000	18.0°N, 112.5°E	Yes
6	22 Nov 2000	20 Dec 2000	24 Jan 2001	20.5°N, 116.0°E	Yes
7	7 Feb 2001	21 Mar 2001	6 Jun 2001	18.5°N, 113.5°E	Yes
8	21 Nov 2001	26 Dec 2001	22 May 2002	16.5°N, 113.0°E	Yes
9	26 Nov 2003	11 Feb 2004	2 Jun 2004	17.0°N, 111.5°E	Yes
10	9 Jun 2004	18 Aug 2004	29 Sep 2004	21.0°N, 118.0°E	No
11	24 Nov 2004	22 Dec 2004	19 Jan 2005	21.5°N, 115.0°E	Yes
12	23 Nov 2005	15 Feb 2006	12 Apr 2006	19.5°N, 115.0°E	No
13	13 Dec 2006	17 Jan 2007	21 Feb 2007	20.5°N, 115.0°E	Yes
14	7 Nov 2007	2 Jan 2008	14 May 2008	17.5°N, 111.0°E	Yes
15	18 Nov 2009	20 Jan 2010	28 Apr 2010	17.0°N, 112.0°E	Yes
16	21 Nov 2011	25 Jan 2012	6 Jun 2012	16.0°N, 111.5°E	Yes
17	24 Oct 2012	12 Dec 2012	27 Feb 2013	17.0°N, 113.5°E	Yes
18	20 Oct 2013	8 Dec 2013	15 Mar 2014	16.5°N, 113.0°E	Yes
19	4 Mar 2014	13 Apr 2014	21 Jun 2014	19.0°N, 114.0°E	Yes

3. Eddy shedding characteristics

a. Satellite observations

To investigate eddy shedding characteristics, we first examined all prominent KLCES events based on the 23-yr (October 1992–October 2014) AVISO altimeter data. The KLCES events were identified based on patterns of SSH inside and west of the Luzon Strait. Specifically, we use the SSH contours originating from the region east of the Luzon Island (north of 17°N and west of 123°E) to denote the path of Kuroshio. When the SSH contours of Kuroshio extend west of 119°E in the northeastern SCS and then bend clockwise back to the Pacific through the northern Luzon Strait, we define it as the occurrence of a KLC event (e.g., purple dashed line in Fig. 1). An AE is thought to form if the enclosed SSH contours with a positive SLA center are found within the KLC and the diameter of its outermost enclosed SSH contour is larger than 100 km. If the SSH contours of AE are totally disconnected from those of the Kuroshio, we consider the AE being detached or shed from the KLC and that the KLC stage ends. In this study, only the prominent events during which both KLC and AE's lifespans are longer than 4 weeks are retained for analysis. Here, the lifespan of the AE is defined as the duration between its shedding time and demise time when its central SLA becomes lower than 5 cm. It should be noted that in the above identification processes, relatively strict criteria are chosen (i.e., 100 km, 4 weeks, and 5 cm) so that the identified KLCES events are not contaminated by errors of the AVISO SLA and SSH (Fu et al. 2010; Chelton et al. 2011; Xiu et al. 2010).

Through examining nearly 8400 altimeter SSH and SLA maps between October 1992 and October 2014, a total of 19 prominent KLCES events were identified. Information of these events, including the start and end dates of KLC and AE, the demise location of AE, and whether a trailing CE is generated to the northeast of AE, is given in Table 1.

During the observational period between April 2011 and June 2014, four prominent KLCES events were captured by our moorings (16–19 in Table 1). Figure 2 shows examples of SSH evolution during the first three of these events (No.16–18). For brevity, the AEs in KLCES events 16–18 are called AE₁₆, AE₁₇, and AE₁₈, respectively, hereinafter. In all three cases, the KLC was clearly seen in the region southwest of Taiwan before the AE was shed, with the Kuroshio first intruding into the SCS through the mid-Luzon Strait and then retro-reflecting back to the Pacific along the southern tip of Taiwan (Figs. 2a,d,g). The westward extension of KLC sometimes reached as far as 117°E (e.g., Fig. 2a), and its duration could last for more than 3 months (e.g., 2 and 4 in Table 1). After the AE was shed, the Kuroshio returned to its leaping path, and a low SSH center (i.e., a CE) tended to occupy the region between the AE and Taiwan (Figs. 2c,f,i). The abovementioned behaviors of Kuroshio path also applied to the other KLCES events listed in Table 1. It is worth noting that among the 19 events there were 17 times a CE was generated to the northeast of AE after it was shed (Table 1), indicating a close connection between the CE and KLCES. Our present finding is consistent with the previous statistical study that AE and CE often coexist in the region southwest of Taiwan (Nan et al. 2011b). From Table 1,

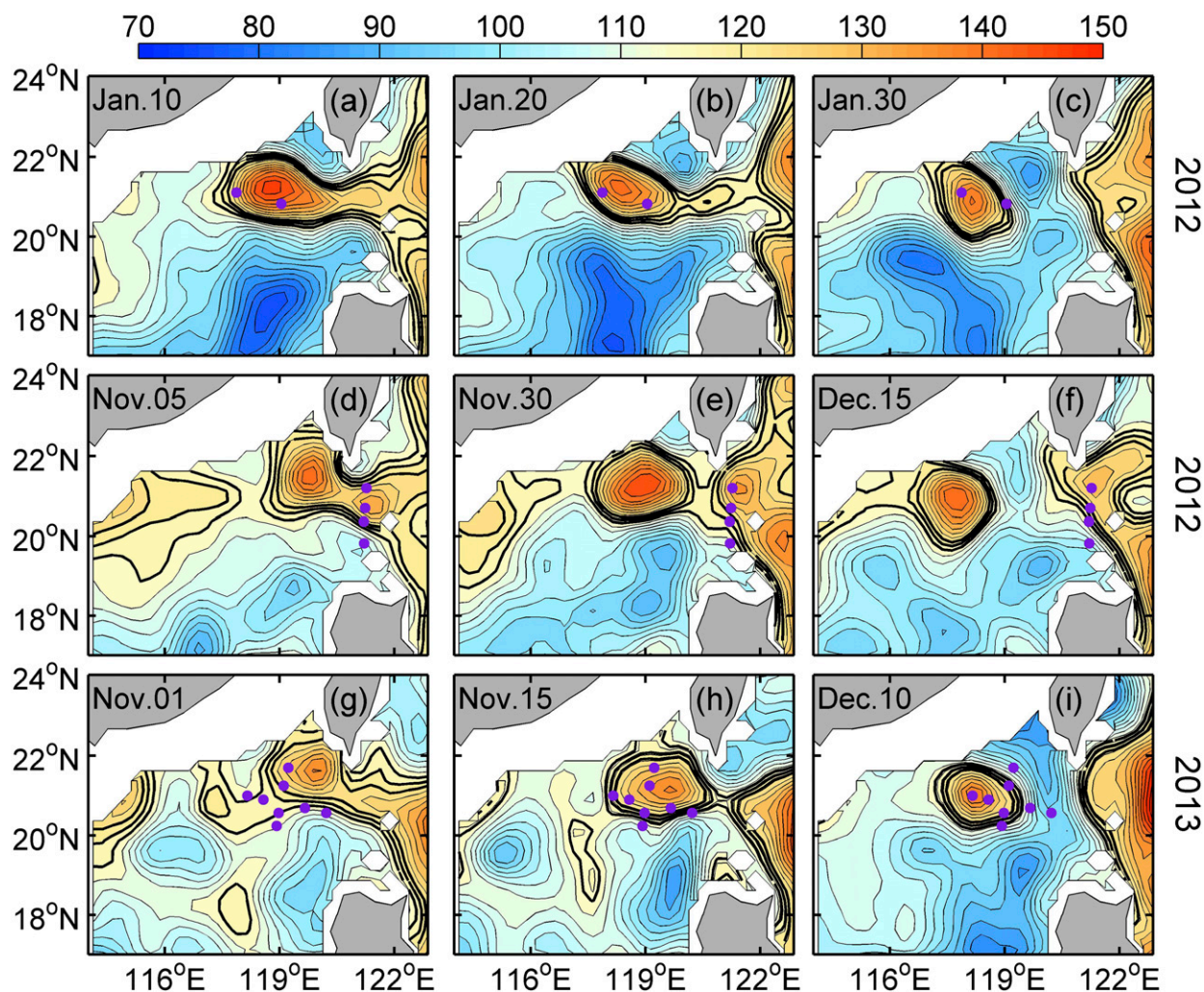


FIG. 2. Altimeter SSHs (cm) in the northeastern SCS during KLCES events (top) 16, (middle) 17, and (bottom) 18. Black lines are SSH contours with an interval of 3 cm. The black thick lines indicate the contours of 117, 120, and 123 cm, which are used to roughly denote the path of Kuroshio. Regions shallower than 100 m are masked by white shading. Purple dots in each panel denote the respective mooring locations shown in Fig. 1. The date (month and day) of each SSH map is shown in top-left corner.

we can also find that except for the event 10, all the KLCES events occur in autumn and winter from September to March. The notable seasonality of KLCESs was suggested to be associated with the northeast monsoon (Jia and Chassignet 2011; Wu and Hsin 2012), and this will be further discussed in section 5.

Considering that the AVISO gridded SSH maps are obtained through interpolating and merging multi-satellite along-track data (Fu et al. 2010; Qiu et al. 2016), one may question whether the AVISO SSH maps can effectively resolve the KLCs and eddies. It is therefore helpful to validate the altimeter-derived results by examining other high-resolution satellite and in situ data. Figure 3 shows the distributions of MODIS 4-km SST and CHL during the KLCES event between November

2011 and February 2012 (event 16 in Table 1). In late November and early December 2011, abnormally high SST and low CHL were found southwest of Taiwan (Figs. 3a,c). Because the Kuroshio water originating from the low-latitude western Pacific is warmer and more oligotrophic compared with the northeastern SCS water, this result validates the existence of KLC as inferred from the altimeter SSH data (black lines in Figs. 3a,c). After AE₁₆ was shed in early February 2012, a CE with negative SLA contours appeared between the AE and Taiwan Island (purple lines in Figs. 3b,d). In contrast to AE₁₆, water within the CE exhibited low SST and high CHL (Figs. 3b,d). This is likely because the CE had trapped colder, fresher, and nutrient-richer water from the nearshore region (Zhang

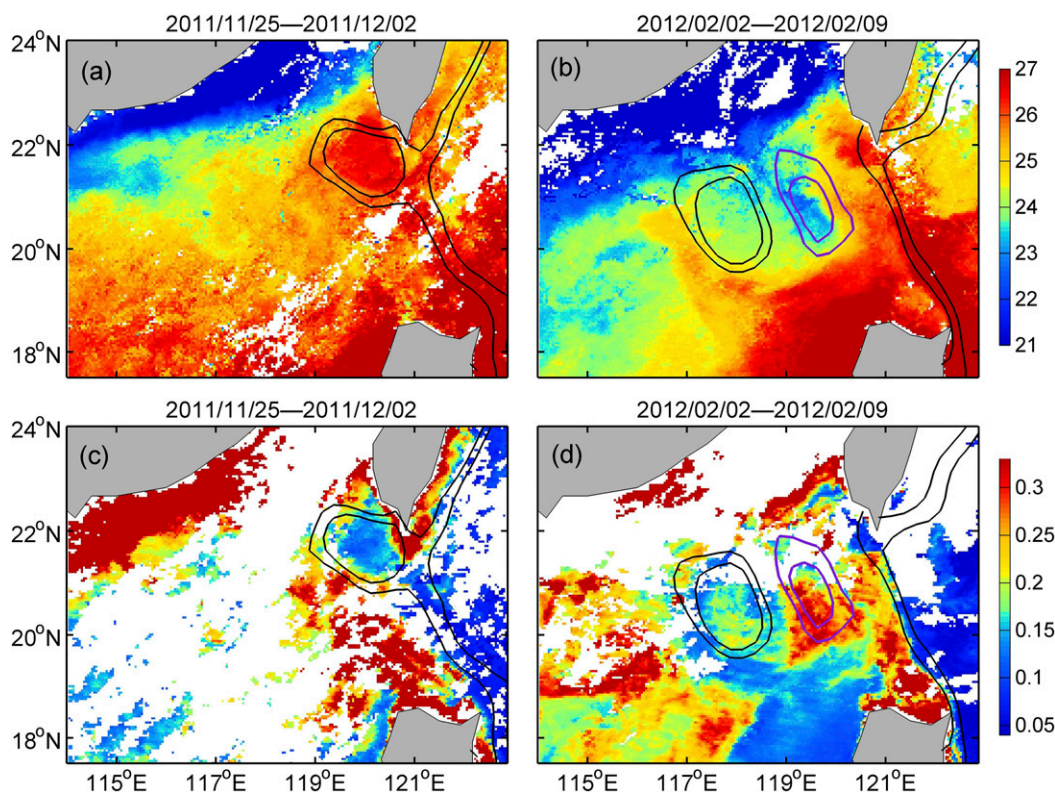


FIG. 3. Maps of MODIS 8-day composite (top) SST ($^{\circ}\text{C}$) and (bottom) surface CHL concentration (mg m^{-3}) in the northeastern SCS and western Pacific during KLCES event 16. White areas indicate bad data retrieval due to the clouds. Two black lines denote the 117- and 123-cm contours of 8-day-averaged SSH during the same period. The -9 - and -15 -cm SLA contours (purple lines) are also shown to indicate the CE. Date of the SST and CHL maps is shown on the top of each panel.

et al. 2016). As revealed from Fig. 4, the SST and CHL distributions for KLCES event 17 had similar characteristics as the event 16, also showing high (low) SST and low (high) CHL within the KLC (CE). We should note that the Kuroshio, which showed strong northwestward (northeastward) velocities in the central (northern) part of the Luzon Strait (purple arrows in Fig. 4), was well observed by our moorings in April 2012–April 2013. Corresponding to the KLC, the zonal (meridional) velocity component was much larger (smaller) than that when the Kuroshio displayed a leaping path across the Luzon Strait (Fig. 4a vs Fig. 4b). The outflow associated with KLC from the SCS to the Pacific can also be confirmed by the low-SST and high-CHL tongue south and southeast of Taiwan (Figs. 4a,c). These results demonstrate that the behavior of Kuroshio before AE's shedding is indeed an inflow–outflow Loop Current in the strait, not just an anticyclonic intrusion (only inflow in the strait) as argued by Yuan et al. (2006). Based on the above validations, we suggest that the KLCES and CE events seen in the AVISO data are robust.

b. Water mass characteristics

As we can see from Fig. 2, AE₁₆ and AE₁₈ were well captured by our mooring arrays in the region southwest of Taiwan, providing a good opportunity to study their water mass characteristics. To pursue this, we first compare the T – S characteristics between the typical Kuroshio water and northeastern SCS water (gray and black lines in Fig. 5). The notable difference between these two water masses is that the Kuroshio water is warmer and saltier in the upper layer (<300 m) but colder and fresher in the intermediate layer (300–1000 m). For the Kuroshio (northeastern SCS) water, its upper-layer salinity maximum and intermediate-layer salinity minimum can reach 34.85 and 34.3 psu (34.6 and 34.4 psu), respectively. To explore the water mass characteristics of AEs, we also plot the mean T – S values within the AEs obtained from moored CTD data (blue and red lines in Fig. 5). Here, the mean T – S values of AEs were computed using moored profiles within the 10-cm SLA contour around the AE's eddy centers

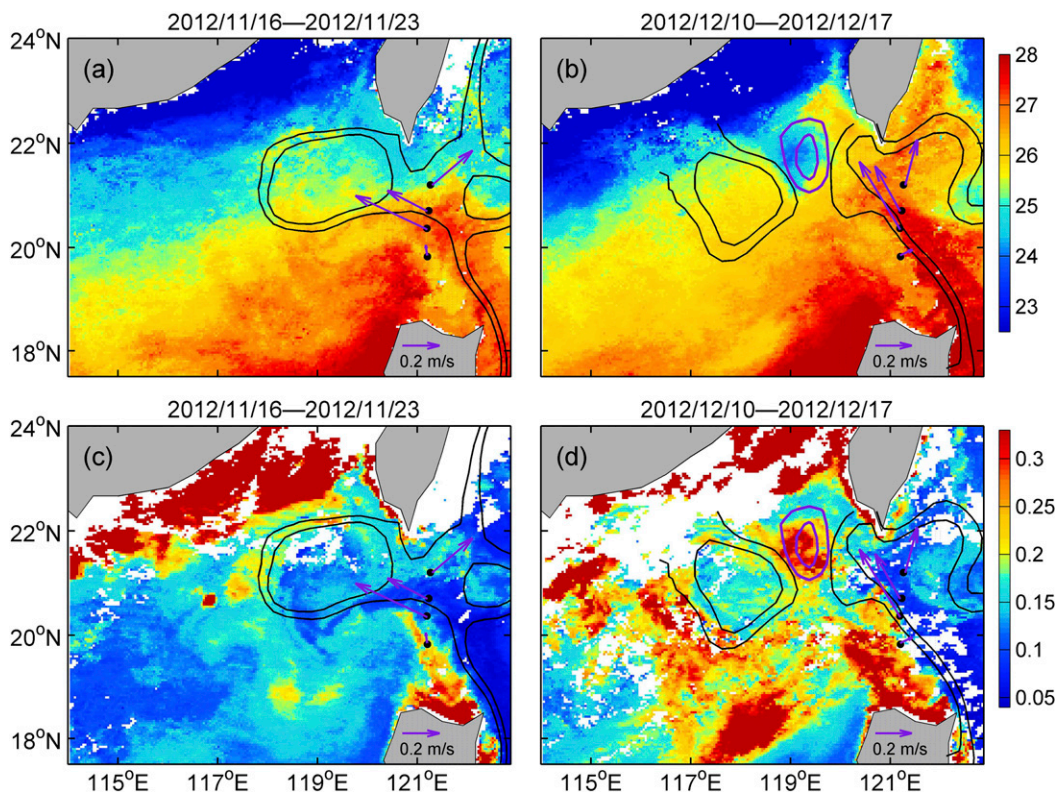


FIG. 4. As in Fig. 3, but for KLCES event 17. Unlike in Fig. 3, purple lines here denote the -3 - and -6 -cm contours of SLA. Purple arrows denote the upper 300-m-averaged current velocity observed by mooring ADCPs.

(Zhang et al. 2016). In the upper layer, the water within both AE₁₆ and AE₁₈ shows T - S properties close to the Kuroshio water, warmer and saltier than the northeastern SCS water. The maximum salinity of their mean T - S values reaches 34.77 and 34.72 psu, respectively. This result again verified the satellite observations that the AEs were shed from KLC. The reason why upper-layer salinity of AEs is lower than the Kuroshio water is likely twofold. First, the KLCs might have entrained some SCS water during their shedding processes. Second, because of the strong tide-induced diapycnal mixing in the Luzon Strait (Tian et al. 2009; Yang et al. 2016), the Kuroshio water might have undergone significant water mass transformation during its transit across the strait. In contrast to the upper layer, the intermediate-layer water within AEs shows no T - S difference with the northeastern SCS water. This result implies that the water mass shedding of Kuroshio is primarily confined to the upper ~ 300 m. Water within the fourth observed AE (during the KLCES event 19) shows similar T - S characteristics as the AE₁₆ and AE₁₈ (figure not shown). Recently, our study has reported the full-depth, three-dimensional (3D) structure of AE₁₈ and found that its velocity signal can extend from the

surface to near the sea bottom, with a depth of ~ 3000 m (Zhang et al. 2016). The deep velocity signal of the AE is in response to the pressure anomaly caused by the upper-layer mass loading, which does not contradict the AE's T - S structures presented in Fig. 5.

Since the AEs are demonstrated to be shed from the KLC, it is meaningful to estimate how much water is brought into the SCS by the shed eddies and evaluate its contribution to the Luzon Strait transport. In this study, we use AE₁₈, which was fully captured by our mooring array (consisting of eight moorings), as a typical case to estimate the volume transport caused by the KLCES. To calculate the volume of Pacific water trapped within AE₁₈, we constructed its 3D structure of salinity anomaly (SA; Fig. 6) following the procedure described in Zhang et al. (2016). The SA profiles were calculated by subtracting the mean salinity profile, which is the averaged profile when moorings are outside of eddies, from the original moored salinity profiles. The calculation was conducted on isopycnic surfaces σ_0 in order to remove the effect of isopycnal heaving caused by oceanic adiabatic motions. As shown in Fig. 6, the area within AE₁₈ is mostly filled with positive SAs. The largest SAs occur around the center of AE₁₈ but not

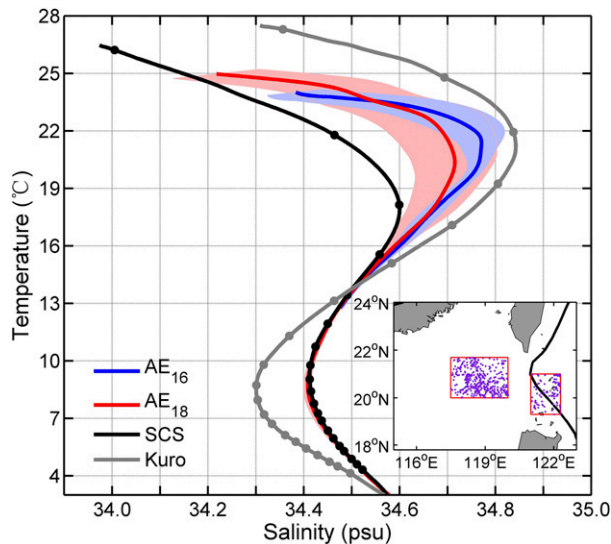


FIG. 5. Mean T - S diagrams of water mass within and outside of the eddies. Blue and red lines show the results within AE_{16} and AE_{18} , respectively, obtained from the moored CTD data. Shadings denote the standard deviations of the T - S . Black and gray lines show the results of the northeastern SCS water and the Kuroshio water, respectively, computed based on historical Argo T - S profiles within the red boxes of the inset figure. The dots on the T - S curves indicate the depths of 50, 100, 150, and 200 m, and so on. Purple dots in the inset figure indicate Argo profiles' locations, and the black curve roughly denotes the axis of the time-mean Kuroshio.

along its peripheries. The SA distribution suggests that during the KLCES event, not only does the Kuroshio front intrude into the SCS, but a significant amount of Pacific water is also brought into the SCS accompanying the eddy shedding. Similar isopycnic salinity distributions during the KLCES events can also be seen from the simulated results of OGCM for the Earth Simulator (OFES; see Figs. S3 and S4 in the supplementary materials).

On each specific σ_0 surface, we also computed the standard deviation of moored salinity values S_{std} outside of the eddies. A water particle is thought to come from the Pacific only if its SA is larger than S_{std} . In other words, we define the SA contour with value of S_{std} as the “eddy edge” of AE_{18} (black dashed line in Fig. 6), inside of which the water is thought to originate from the Pacific. Figures 7a and 7b show the profiles of averaged SA within AE_{18} and radius of the eddy edge with an equal area to circle, respectively. The averaged SA (radius) shows its largest value of 0.23 psu (135 km) in the uppermost layer ($23.5\sigma_0$) and gradually decreases with an increasing σ_0 . At the layer of $\sigma_0 = 26.0 \text{ kg m}^{-3}$, the SA minus its standard deviation becomes close to zero. This layer is therefore defined as the bottom of KLC water

mass. By integrating AE_{18} 's area with depth from its bottom to surface, the mean volume of $1.44 \times 10^{13} \text{ m}^3$ is obtained. Because that, in the above calculation, water within AE_{18} is presumed to totally come from the Pacific, this volume should be the upper bound of Pacific water volume brought into the SCS by AE_{18} . If we assume that water within AE is a mixture between the SCS and Pacific waters (as mentioned above, the reduced salinity of AE in Fig. 5 may also be due to strong diapycnal mixing), we can roughly estimate the percentage of Pacific water a trapped within AE using $S_{AE} = aS_{Paci} + (1 - a)S_{SCS}$, where S_{AE} , S_{Paci} , and S_{SCS} denote the salinity of AE, Pacific, and SCS waters, respectively. Substituting the salinities in Fig. 5 into this formula reveals that $a = 62\%$ of the mixed water within AE comes from the Pacific. Because the diapycnal mixing is not considered above, this percentage should be a lower bound. Therefore, a reasonable range for the volume of Pacific water trapped within AE_{18} should be $Vol = 0.89\text{--}1.44 \times 10^{13} \text{ m}^3$. This result is nearly one order larger than that ($2 \times 10^{12} \text{ m}^3$) estimated by Jia and Chassignet (2011) based on time-integrated Ekman transport during winter season, suggesting that the Ekman drift caused by the northeast monsoon is not the dominant mechanism for KLCES. If we assume that all 19 KLCESs in Table 1 trap the same volume of Pacific water, it gives rise to an equivalent annual-mean volume transport of $19 \times Vol/23 \text{ years} = 0.23\text{--}0.38 \text{ Sv}$ ($1 \text{ Sv} \equiv 10^6 \text{ m}^3 \text{ s}^{-1}$). The KLCES-caused volume transport roughly accounts for 6.6%–10.8% of the annual-mean Luzon Strait transport in the upper layer [3.5 Sv; see a summary in Xu and Oey (2014)].

4. Mechanisms of eddy shedding

In this section, we explore the eddy shedding mechanism of KLC through analyzing the altimeter-based composite result and HYCOM-based eddy energetics.

a. Composite result

Figure 8 shows the composite SSH and SLA maps for the historical KLCES events with dt indicating the weeks relative to the date of eddy shedding. The composite result is obtained based on the 17 KLCES events listed in Table 1 that have an accompanying CE. Nine weeks before AE's shedding, the KLC with semi-enclosed SSH contours and positive SLAs begin to form southwest of Taiwan ($dt = -9$; Fig. 8b). The KLC subsequently grows and expands southwestward. With the expansion of KLC, negative SLAs begin to appear between KLC and Taiwan at $dt = -3$ (Fig. 8e). After that, the negative SLA center quickly strengthens and squeezes the north branch of KLC ($dt = -1$; Fig. 8f). At

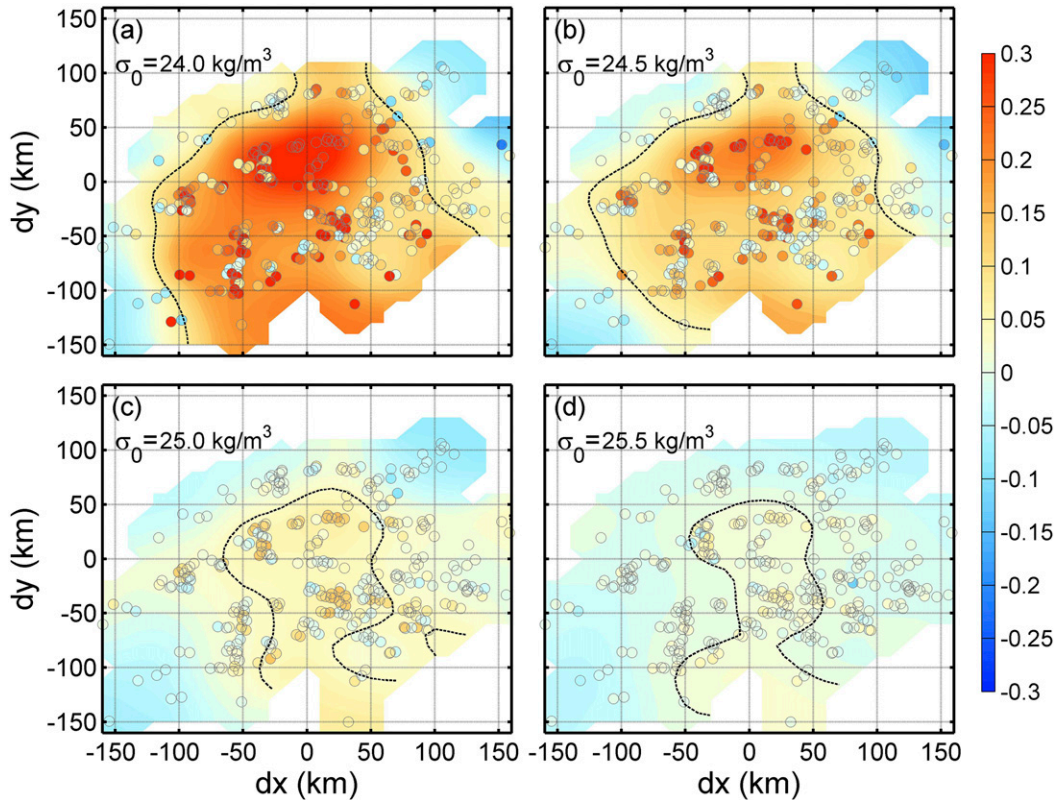


FIG. 6. Distribution of SAs within and around AE₁₈ under an eddy center coordinate system. Results shown on the isopycnic surfaces of (a) 24.0, (b) 24.5, (c) 25.0, and (d) 25.5 kg m⁻³. The gray-edged colorful dots show the original SAs, and the shadings show the results obtained by objective interpolation. The black dashed line denotes the SA contour with a value of S_{std} , where S_{std} is the standard deviation of the moored salinities outside of eddies.

$dt = 0$ and $dt = 1$, the negative SLA center develops into a prominent CE with the SLA center reaching -15 cm (Figs. 8g,h). This composite result is consistent with the aforementioned eddy pair pattern southwest of Taiwan (Figs. 2–4). Because of the southward expansion of CE, the neck of KLC is pinched off, finally resulting in the detachment of AE from KLC. Notice that the shedding process of KLC is also accompanied by the growth of the low-SLA region northwest of Luzon (Figs. 8d–i). The northward expansion of this low-SLA region (another CE) may also contribute to the detachment of AE. The above scenario is very similar to that for the Loop Current Eddy shedding process in the Gulf of Mexico, which is also featured with CEs on both sides of the Loop Current (e.g., Schmitz 2005; Oey 2008).

b. Generation mechanism of CE

From Fig. 8, it is indicated that the generation and growth of CE southwest of Taiwan results in the detachment of AE from the KLC. Next we investigate the generation mechanism of the CE in terms of eddy

energetics and hydrodynamic instability. To clarify the dominant energy source for the CE, we plot in Fig. 9 the composite baroclinic (BC) and barotropic (BT) eddy energy conversion rates and rate of wind stress work (WW) for KLCES events 16–18. Here, BC, BT, and WW are defined, respectively, as below:

$$BC = - \int \frac{g^2}{\rho_0 N^2} \overline{\mathbf{v}'\rho'} \cdot \nabla_h \bar{\rho} dz, \quad (1)$$

$$BT = - \int \rho_0 \frac{\partial \bar{u}_i}{\partial x_j} \overline{u'_i u'_j} dz, \quad \text{and} \quad (2)$$

$$WW = \overline{\boldsymbol{\tau}_w \cdot \mathbf{v}'_0}. \quad (3)$$

In the above equations, overbars and primes denote time mean (1 month) and anomalies from the time mean, respectively; g is the gravity; N is the buoyancy frequency; $\boldsymbol{\tau}_w$ and \mathbf{v}'_0 denote the wind stress and surface horizontal velocity, respectively; $\rho_0 = 1030 \text{ kg m}^{-3}$ is the mean seawater density; summations over the repeated indices i and j are used in Eq. (2); and the other symbols and notations are standard. Physically, a positive BC

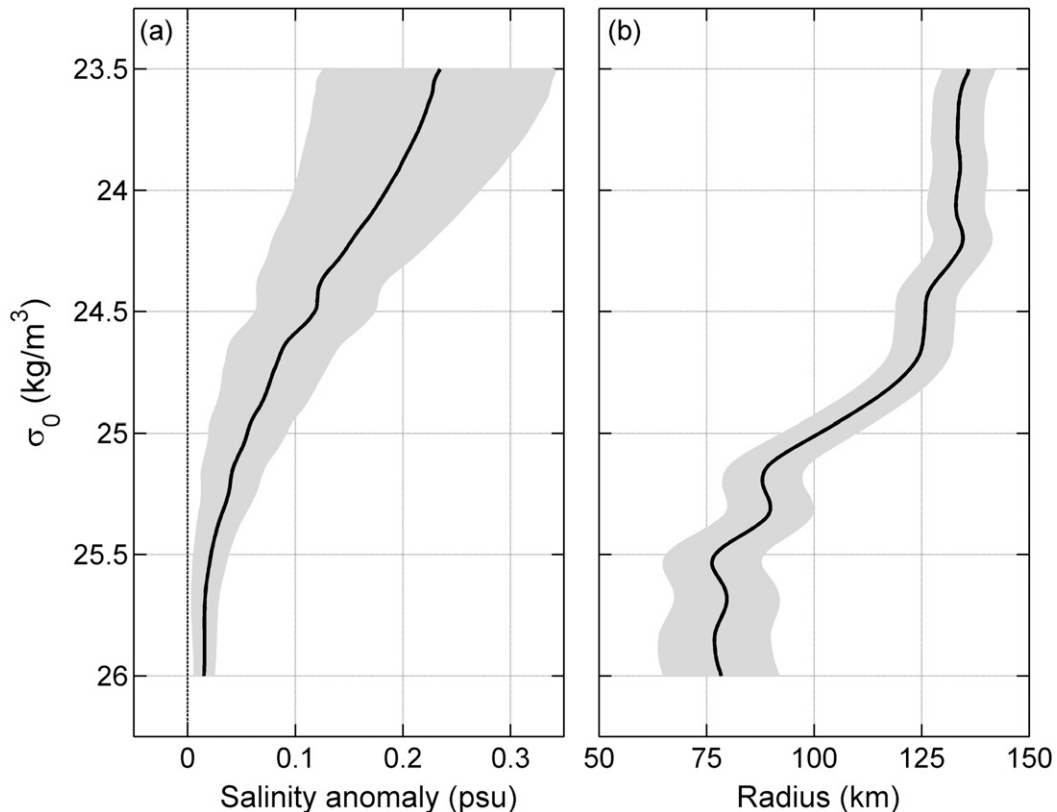


FIG. 7. (a) Vertical profile of area-averaged SA within AE_{18} (black solid line). Here, the S_{std} contour as shown in Fig. 6 is defined as the edge of AE_{18} . Gray shading denotes the standard deviation of SA within AE_{18} . (b) Vertical profile of AE_{18} 's radius (black line), which is represented by the radius of an equal area circle on each isopycnal surface. Gray shadings denote the standard deviations associated with the black line.

(BT) means mean potential energy (kinetic energy) transferring to eddy potential energy (kinetic energy) and is the cause for baroclinic (barotropic) instability. Depth integrals for BC and BT in Fig. 9 are from 200 m to the sea surface. The periods used to calculate the time mean are over 25 December 2011–25 January 2012, 12 November 2012–12 December 2012, and 8 November 2013–8 December 2013, respectively, for the three KLCES events (see Figs. 10b–d).

From the composite SLA and SSH distributions, the well-defined KLC and an embryo CE can be clearly seen southwest of Taiwan (Fig. 9a). This again demonstrates the success of HYCOM in simulating the KLCES events. In the regions of embryo CE and the north branch of KLC, there are strong positive BTs as revealed from Fig. 9c. Compared to BT, BC and WW in the CE region are much weaker and dominated by negative values (Figs. 9b,d). The results in Fig. 9 suggest that the energy source for CE is primarily from barotropic instability of the mean flow, that is, the northern branch of KLC; work done by the local wind stress curl (WSC) plays a minor role.

According to the hydrodynamic instability theory, the necessary condition of barotropic instability for a zonal flow is that the meridional gradient of barotropic potential vorticity (PV) changes sign in the domain (Pedlosky 1987). To examine whether the northern branch of KLC meets the condition of barotropic instability, we plot in Fig. 10 the meridional gradient of barotropic PV, that is, $\beta - U_{yy}$, during four different KLCES events (15–18). Here, β is the meridional gradient of the Coriolis parameter, and U_{yy} is the second derivative of the mean eastward velocity averaged over 1 month and over the upper 200 m (indicated on the maps of Fig. 10). Indeed, strong $\beta - U_{yy}$ with different signs are found in the regions of CE and the northern branch of KLC, agreeing well with the large BT regions revealed in Fig. 9c. The value of $\beta - U_{yy}$ is originally positive between the KLC's center and the axis of eastward KLC (i.e., northern branch of KLC). Because of the strong horizontal velocity shear between the eastward KLC and southwest coast of Taiwan, $\beta - U_{yy}$ sharply changes sign to negative north of the axis of eastward KLC. Actually the meridional distribution

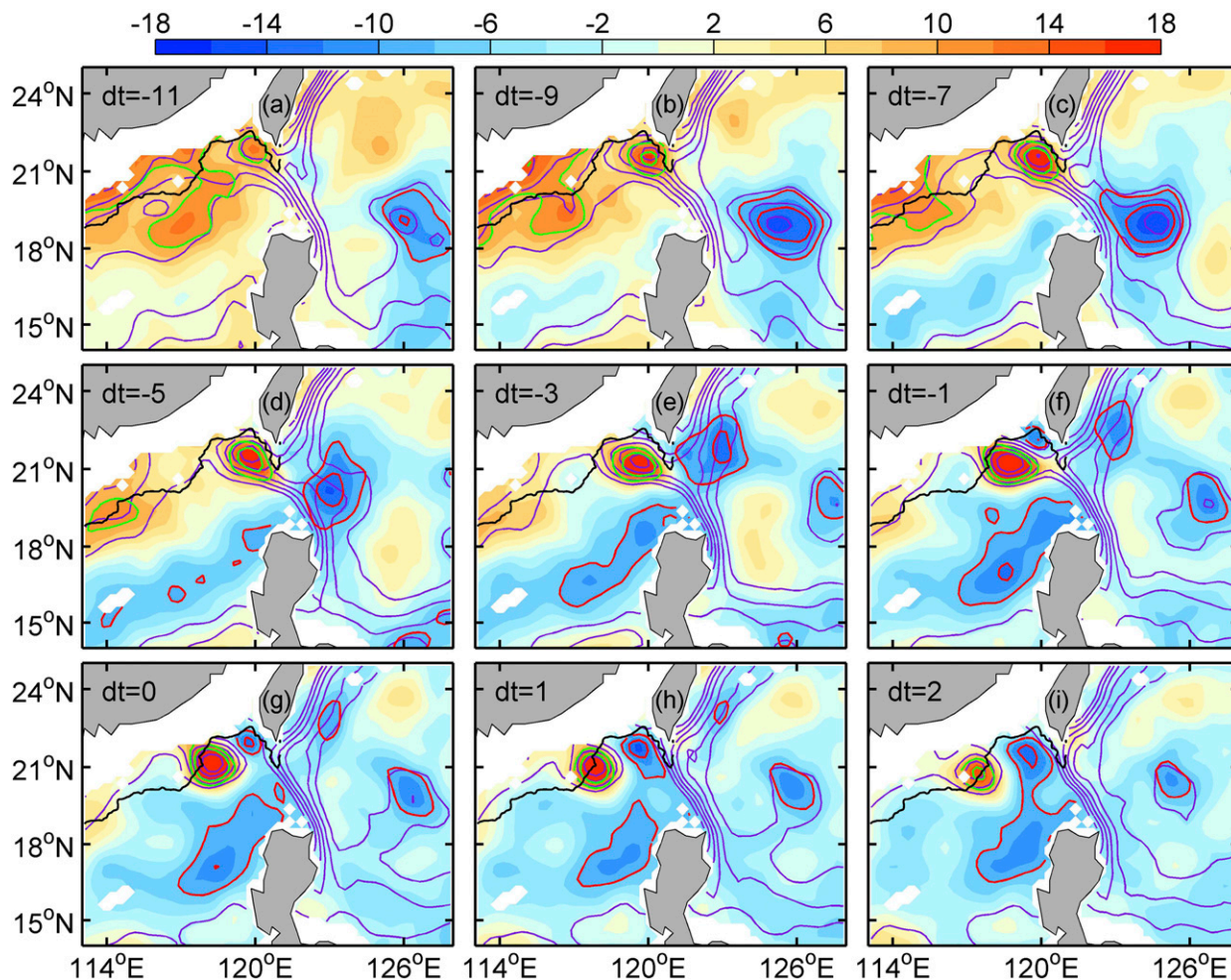


FIG. 8. Composite SLA (shadings; cm) and SSH (purple contours) based on the 17 selected KLCES events. Regions shallower than 100 m are masked by white shading. The dt in top-left corner of each panel denotes the weeks before (negative value) or after (positive value) the AE is shed from the KLC. The time dt = 0 (Fig. 8g) indicates that the AE is just detached from the Kuroshio SSH contours, when its SSH contours begin to isolate themselves from the Kuroshio SSH contours. Green (red) lines denote the 10- and 15-cm (−8 and −12 cm) SLA contours, which indicate the location of AE (CE). Purple lines are the SSH contours ranging from 105 to 130 cm with an interval of 5 cm. The black line indicates the 1000-m isobath.

of $-U_{yy}$ is rather close to $\beta - U_{yy}$ (Fig. 11a), suggesting its dominant role in changing the sign of the PV gradient. The above distribution of $\beta - U_{yy}$ applies to all of the four KLCES events and demonstrates that the northern branch of KLC meets the necessary condition of barotropic instability. The background cyclonic velocity shear associated with the KLC's northern branch and the constraint of PV conservation during its offshore movement (vortex tube stretch) may provide favorable conditions for the growth of cyclonic disturbances and explain why a CE but not an AE is generated during the barotropic instability.

To further investigate the generation of CE, we analyze the stability properties of KLC based on the 1.5-layer reduced-gravity model used in Qiu and Chen

(2004). By numerically solving the eigenvalue problem for barotropic instability of KLC [Eq. (A4); see details in the appendix], we obtain the growth rates kc_i of unstable waves as a function of wavenumber k (Fig. 11b). It shows that the most unstable wave (i.e., the wave that has the largest kc_i) occurs at $k = 1.8 \times 10^{-5} \text{ m}^{-1}$ with the growth rate $kc_i = 7.8 \times 10^{-7} \text{ s}^{-1}$. The corresponding length $1/k$ and time scales $1/kc_i$ of the most unstable wave are 56 km and 15 days, respectively, which are comparable to those of the CE at its growth stage (Figs. 8e–g). The above analysis explains why the CE is quickly generated during the KLC event (with a period of ~30 days) and has a relatively small radius.

To conclude, we schematically summarize in Fig. 12 the generation mechanisms of the AE and CE pair

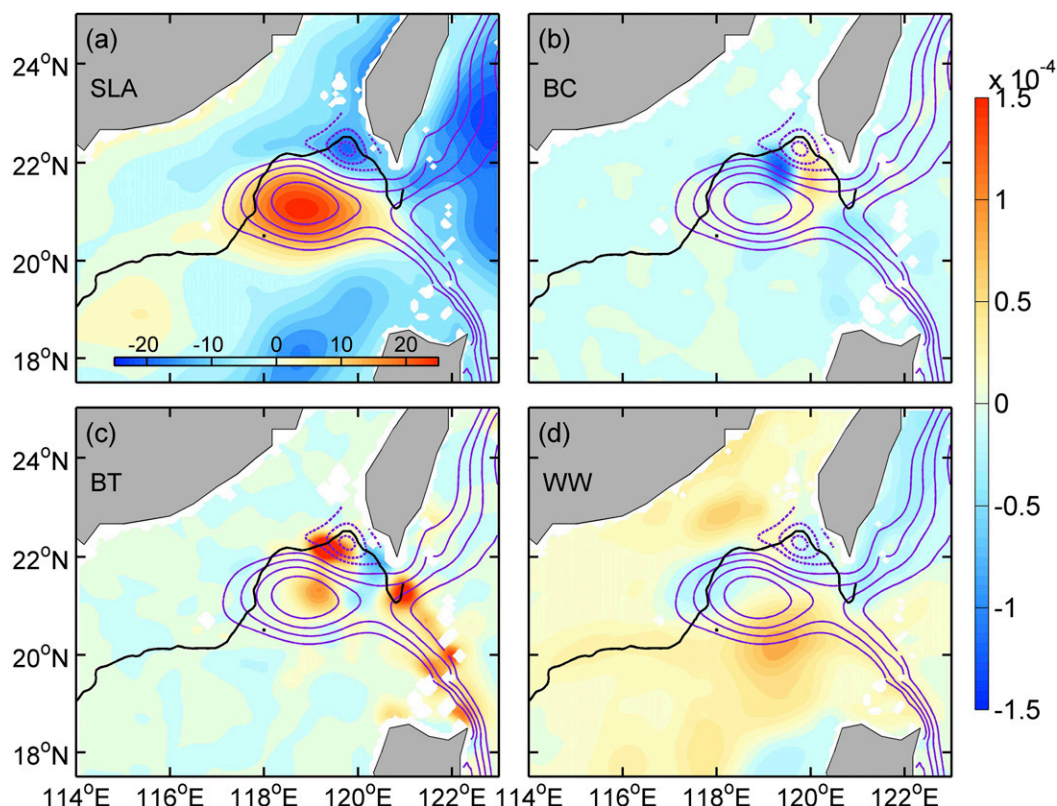


FIG. 9. Composite HYCOM (a) SLA (cm), (b) BC ($\text{m}^3 \text{s}^{-3}$), (c) BT ($\text{m}^3 \text{s}^{-3}$), and (d) WW ($\text{m}^3 \text{s}^{-3}$) for KLCES events 16–18, as depicted in Fig. 2. Purple solid lines are the composite SSH contours ranging from 75 to 90 cm with an interval of 5 cm. Purple dashed lines denote the -9 -, -13 -, and -17 -cm SLA contours, which indicate the location of CE. The black line indicates the 1000-m isobath. Note that the color bars of (a) and (b)–(d) represent different quantities.

associated with KLCES. The large horizontal velocity shear of the northern branch of KLC leads to strong barotropic instabilities southwest of Taiwan, which provide energy to CE for its quick generation and growth. The expansion and migration of CE in turn facilitate the shedding of KLC and result in AE's final detachment. The above relationship between KLC and CE well explains the common occurrence of eddy pairs southwest of Taiwan (Table 1; Nan et al. 2011b).

5. Summary and discussion

Through the synergetic analyses of moored and satellite data and HYCOM products, the present study explored the characteristics and mechanisms of KLCES in the northeastern SCS. In particular, the concurrent in situ and satellite observations between April 2011 and June 2014 provided us with a unique opportunity to explore in detail the development of KLC and the eddy shedding processes southwest of Taiwan. During a KLC event, the Kuroshio first meanders into the SCS through

the mid-Luzon Strait and then it bends clockwise back to the Pacific along the southern tip of Taiwan. Water within the KLC and its detached AE is characterized by high $T-S$ and low CHL in the upper layer. Based on the 23-yr historical altimeter data between October 1992 and October 2014, a total of 19 prominent KLCES events were identified. Compared to the leaping path of Kuroshio, the KLC is a relatively transient phenomenon with its duration (from development to AE's detachment) ranging from 1 to 3 months. The KLCES events are found to have a strong seasonal variation, most of which occur in the northeast monsoon season (i.e., boreal autumn and winter).

Based on the extensive mooring array observations, this study quantified the volume transport caused by KLCES. On average, the AE shedding from KLC can transport 0.23–0.38-Sv Pacific water into the SCS per year, accounting for 6.6%–10.8% of the upper-layer Luzon Strait transport. Given that the Pacific water trapped within the AEs shows large property differences with the SCS water and given that the AEs can have long

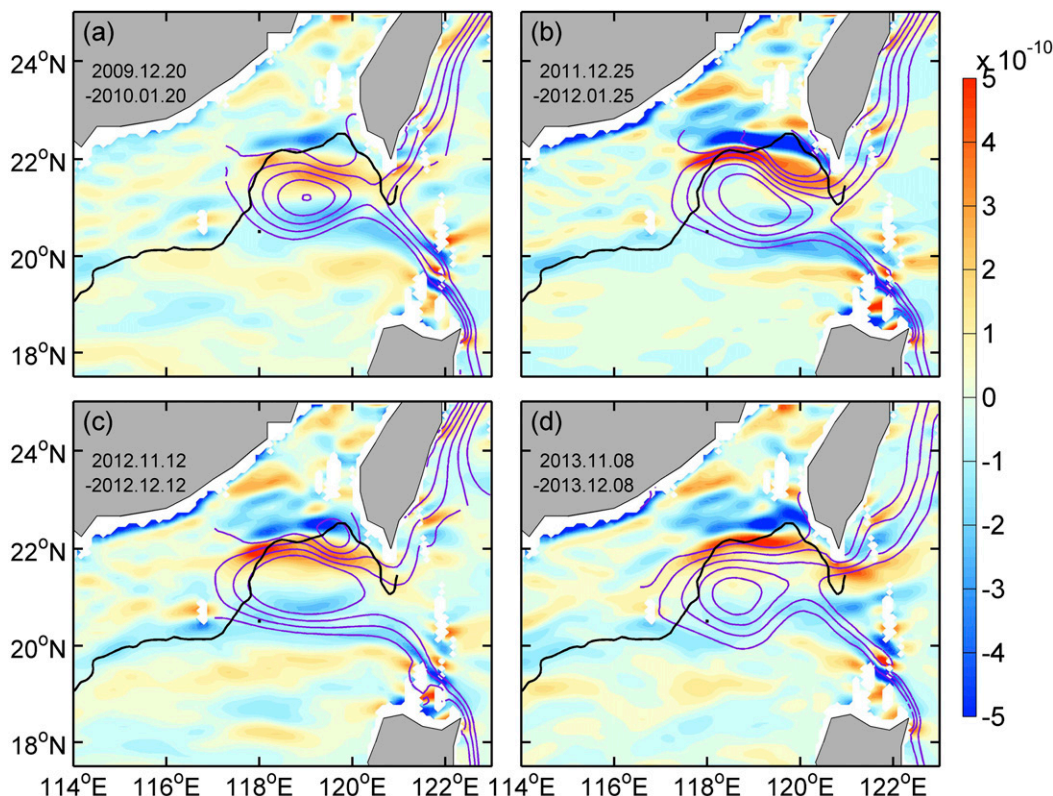


FIG. 10. Spatial distribution of $\beta - U_{yy}$ ($\text{m}^{-1} \text{s}^{-1}$) calculated based on HYCOM data. Purple and black solid lines denote the mean SSH contours and the 1000-m isobath, respectively. The time period used for calculation is also shown on each map.

lifespan and traveling distance after shedding (Table 1), they may exert important influences on the biogeochemical processes in the northern SCS.

Among the historical KLCES events, nearly 90% of them (17 over 19) are accompanied by a CE generated immediately to the northeast of AE. The composite KLCES evolution suggests that the generation and growth of the CE southwest of Taiwan facilitates and finally results in the detachment of AE from the KLC. By analyzing the source of eddy energy and stability of mean flow based on HYCOM products, we find that the CE is primarily generated by barotropic instability of the northern branch of KLC. Because of the large horizontal velocity shear southwest of Taiwan, the most unstable wave of the barotropic instability has a rather large growth rate ($1/kc_i = 15$ days), which explains why the CE can be quickly generated during the relatively short-period KLC event. The above intrinsic relation between KLCES and CE explains the phenomenon that the AE is nearly always accompanied by a CE in the KLCES events southwest of Taiwan. It should be noted that, after the detachment of AE, the leaping Kuroshio in the Luzon Strait has strong cyclonic velocity shear west of its axis

(Figs. 8h,i, 12b). This cyclonic velocity shear may be favorable for the further growth of CE after it is generated.

The present study has focused on the characteristics and mechanisms of KLCES but not how the KLC initially forms and develops. From Fig. 8, we find that the developing process of KLC is accompanied by a strong CE in the western Pacific (Figs. 8a–f). This CE exists originally far to the east of Luzon at $dt = -11$ and gradually propagates westward with time. At $dt = -9$ and $dt = -7$, it approaches the western boundary of the Pacific, beginning to interact with the Kuroshio. Then the CE propagates northward along the leaping path of Kuroshio (Figs. 8d–f) and is finally dissipated east of Taiwan at $dt = 0$. The Kuroshio–CE interaction process can be divided into two stages. At the first stage between $dt = -9$ and $dt = -5$, the strength of the Kuroshio east of Luzon (indicated by intensity of the SSH gradients) is greatly reduced due to the CE, which provides a favorable condition for its intrusion into the SCS according to the nonlinear hysteresis theory (Sheremet 2001; Yuan and Wang 2011). At the second stage between $dt = -3$ and $dt = -1$, the CE moves to southeast and east of Taiwan, which blocks the northward Kuroshio and further

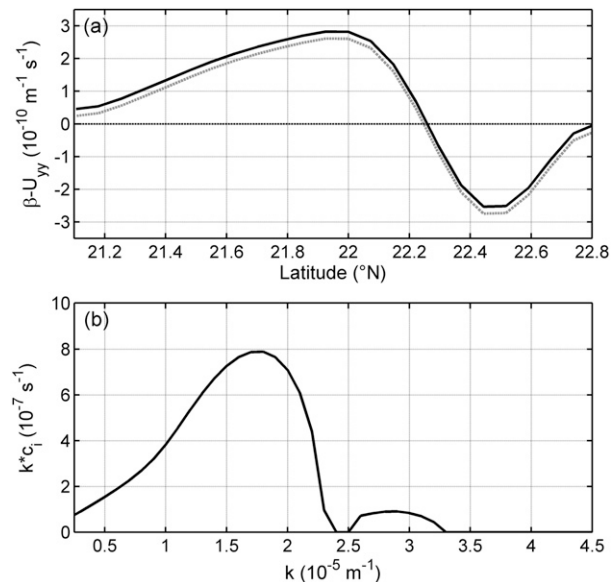


FIG. 11. (a) Meridional distribution of $\beta - U_{yy}$ (solid black) and $-U_{yy}$ (dashed gray) associated with the northern branch of KLC. Here, U_{yy} is averaged between 118.5° and 119.5°E and mean values of the four KLC cases in Fig. 10 are used. (b) Growth rate of barotropic unstable waves as a function of wavenumber k .

facilitates the development of KLC. Based on the above analysis we suggest that the formation and development of KLC can be partially explained by the Kuroshio–CE interaction east of Luzon. To verify this point, however, more focused studies should be conducted in the future.

Previous studies have suggested that the autumn–winter preference of KLCESs may be attributed to the northeast monsoon (Jia and Chassignet 2011; Wu and Hsin 2012). To investigate how monsoon winds influence the loop formation and eddy shedding, we

analyze the KLCES events occurring in two different OFES runs between July 1999 and December 2006. The two OFES runs have the same model configurations except that they use winds from QuikSCAT measurements and National Centers for Environmental Prediction (NCEP) reanalysis, respectively (Qscat run vs NCEP run, hereinafter). The largest difference between the NCEP and observed (i.e., Qscat) winds is that in winter the former is over smoothed and there are no enhanced local WSCs in the lee sides of Taiwan and Luzon Islands (Fig. S2 in the supplementary material). Based on the criteria used in section 3, a total of six and eight prominent KLCES events were identified in Qscat and NCEP runs, respectively, over the 7.5 years (Table S1 in the supplementary material). The slightly larger eddy shedding rate in the NCEP run ($8/7.5$ vs $6/7.5$) indicates that the existence of local WCS southwest of Taiwan is not a necessary condition for KLCES. In fact, the kinetic energy input by WW over the KLC region in 3 months (Fig. 9d) is only $1.4 \times 10^{13} \text{ J}$, which cannot account for the total kinetic energy of AE ($9.8 \times 10^{14} \text{ J}$) directly observed by Zhang et al. (2016).

Although energy input by the local WCS is very minor, it does not mean that the WCS is unimportance for KLCES. By comparing the KLCES events in two OFES runs, it is found that most KLCES events in Qscat run (five out of six) occur in the northeast monsoon season, which is quite similar to the altimeter observations; for the NCEP run, however, the occurrence of KLCESs does not show an obvious seasonal variation (Table S1). Because the wind magnitudes and WCSs in summer and wind magnitudes in winter are similar for Qscat and NCEP runs (Fig. S2), the large difference between KLCESs in these two runs manifests the importance of

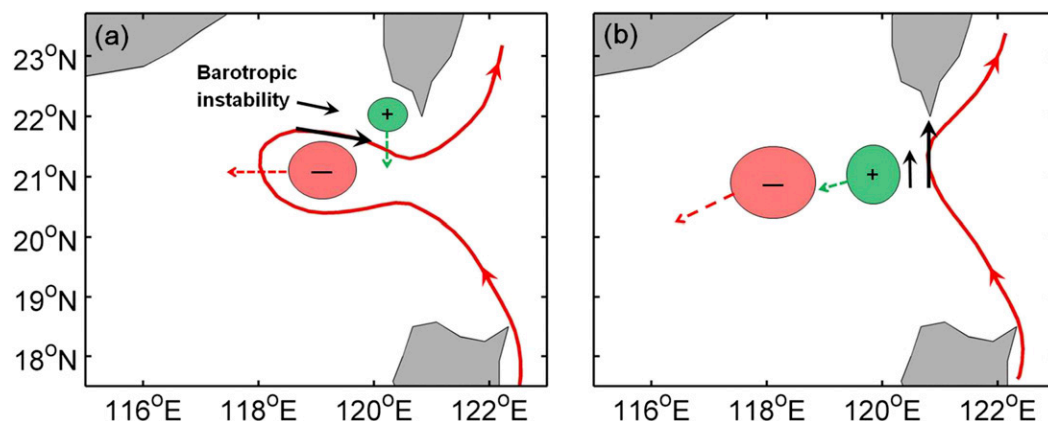


FIG. 12. Schematic diagram of generation mechanisms of the AE and CE southwest of Taiwan. Red curve denotes the axis of the Kuroshio and black arrows denote horizontal velocity shear associated with the Kuroshio. The AE (CE) and its migration direction are marked by red (green) circle and dashed line arrow, respectively. The stages (a) before and (b) after the AE shedding are shown.

local WCSs for KLCES's preferred occurrence in autumn and winter. The reason is likely because the negative WCS southwest of Taiwan provides negative vorticity to the surface and near-surface current that further helps the development of KLC (Wu and Hsin 2012). It is also worth mentioning that in both the Qscat and NCEP runs a CE is generated southwest of Taiwan during the KLCES event that seems to facilitate the detachment of AE from KLC (Fig. S2 and Fig. S3). This result supports our conclusion that the CE is primarily generated through barotropic instability of the KLC but not the vorticity or energy input from the local WCS southwest of Taiwan.

Acknowledgments. The authors express their sincere thanks to two anonymous reviewers for the constructive comments to the earlier manuscript. The help provided by Dr. Shuiming Chen from the University of Hawai'i at Mānoa in numerically solving the eigenvalue problem is also appreciated. This work is jointly supported by National Key Basic Research Program of China (Program 973; Grant 2014CB745000), the National Natural Science Foundation of China (Grants 41506011 and 41576009), the National High Technology Research and Development Program of China (Grants 2013AA09A502 and 2013AA09A501), the Foundation for Innovative Research Groups of the National Natural Science Foundation of China (Grant 41521091), the NSFC-Shandong Joint Fund for Marine Science Research Centers (Grant U1406401), Global Change and Air–Sea Interaction Project (Grants GASI-03-01-01-03 and GASI-IPOVAI-01-03), and a grant from Sanya Institute of Deep-Sea Science and Engineering (SIDSSE-201207).

APPENDIX

Deducing the Eigenvalue Problem for Barotropic Stability Analysis

Considering that the KLC is active only upon the upper several hundred meters, the 1.5-layer reduced-gravity model is adopted here to study its barotropic instability problem. For a mean sheared zonal flow $U(y)$ in the upper active layer, the linearized momentum and continuity equations governing the perturbation velocity \mathbf{u}' and upper-layer thickness h' are

$$\frac{\partial \mathbf{u}'}{\partial t} + U \frac{\partial \mathbf{u}'}{\partial x} + v' \frac{\partial U}{\partial y} \mathbf{i} + f \mathbf{k} \times \mathbf{u}' = -g' \nabla h', \quad \text{and} \quad (\text{A1})$$

$$\frac{\partial h'}{\partial t} + U \frac{\partial h'}{\partial x} + v' \frac{\partial H}{\partial y} + H \nabla \cdot \mathbf{u}' = 0, \quad (\text{A2})$$

where g' is the reduced gravity (a constant), and H is the mean upper-layer thickness, which is in geostrophic balance with U through $fU = -g'H_y$. Cross differentiating the zonal and meridional component of the momentum equations (A1) and substituting the $\nabla \cdot \mathbf{u}'$ term with (A2) gives rise to the PV equation

$$\left(\frac{\partial}{\partial t} + U \frac{\partial}{\partial x} \right) q + v' \frac{\partial Q}{\partial y} = 0, \quad (\text{A3})$$

where $Q = (f - U_y)/H$ and $q = (1/H)[(\partial v'/\partial x) - (\partial u'/\partial y)] - (h'/H)Q$ are the mean and perturbation PVs, respectively. With assumption that the perturbation motions are quasigeostrophic ($f \mathbf{k} \times \mathbf{u}' = -g' \nabla h'$), we can seek the normal-mode solution {i.e., $h' = \text{Re}[A \exp ik(x - ct)]$ } of Eq. (A3) and obtain

$$\frac{d^2}{dy^2} A - (k^2 + \lambda_d^{-2}) A + \frac{\beta - U_{yy} + U \lambda_d^{-2}}{U - c} A = 0. \quad (\text{A4})$$

This is the eigenvalue problem for barotropic stability analysis of the horizontally sheared flow $U(y)$ if c is regarded as the eigenvalue. Here, $\lambda_d = \sqrt{g'H/f}$ is the first baroclinic Rossby radius of deformation, and $g' = 0.03 \text{ m s}^{-2}$ and $H = 200 \text{ m}$ are used in this study according to G. Wang et al. (2008). With respect to $U(y)$ and U_{yy} , the mean values of the four KLC cases in Fig. 10 averaged between 118.5° and 119.5°E (see Fig. 11a for U_{yy}) are used.

REFERENCES

- Alford, M. H., and Coauthors, 2015: The formation and fate of internal waves in the South China Sea. *Nature*, **521**, 65–69, doi:10.1038/nature14399.
- Caruso, M. J., G. G. Gawarkiewicz, and R. C. Beardsley, 2006: Interannual variability of the Kuroshio intrusion in the South China Sea. *J. Oceanogr.*, **62**, 559–575, doi:10.1007/s10872-006-0076-0.
- Centurioni, L. R., P. P. Niiler, and D. K. Lee, 2004: Observations of inflow of Philippine Sea surface water into the South China Sea through the Luzon Strait. *J. Phys. Oceanogr.*, **34**, 113–121, doi:10.1175/1520-0485(2004)034<0113:OOIOPS>2.0.CO;2.
- Chelton, D. B., M. G. Schlax, and R. M. Samelson, 2011: Global observations of nonlinear mesoscale eddies. *Prog. Oceanogr.*, **91**, 167–216, doi:10.1016/j.pocean.2011.01.002.
- Chen, G., Y. Hou, and X. Chu, 2011: Mesoscale eddies in the South China Sea: Mean properties, spatiotemporal variability, and impact on thermohaline structure. *J. Geophys. Res.*, **116**, C06018, doi:10.1029/2011JD016244.
- Farris, A., and M. Wimbush, 1996: Wind-induced Kuroshio intrusion into the South China Sea. *J. Oceanogr.*, **52**, 771–784, doi:10.1007/BF02239465.
- Fu, L.-L., D. B. Chelton, P.-Y. Le Traon, and R. Morrow, 2010: Eddy dynamics from satellite altimetry. *Oceanography*, **23**, 14–25, doi:10.5670/oceanog.2010.02.

- Guo, J.-S., Y. Feng, Y.-L. Yuan, and B.-H. Guo, 2013: Kuroshio Loop Current intruding into the South China Sea and its shedding eddy (in Chinese with English abstract). *Oceanol. Limnol. Sin.*, **44**, 537–544.
- Huang, X., Z. Chen, W. Zhao, Z. Zhang, C. Zhou, Q. Yang, and J. Tian, 2016: An extreme internal solitary wave event observed in the northern South China Sea. *Sci. Rep.*, **6**, 30 041, doi:10.1038/srep30041.
- , Z. Zhang, X. Zhang, W. Zhao, and J. Tian, 2017: Impacts of a mesoscale eddy pair on internal solitary waves in the northern South China Sea revealed by mooring array observations. *J. Phys. Oceanogr.*, doi:10.1175/JPO-D-16-0111.1, in press.
- Jia, Y., and Q. Liu, 2004: Eddy shedding from the Kuroshio bend at Luzon Strait. *J. Oceanogr.*, **60**, 1063–1069, doi:10.1007/s10872-005-0014-6.
- , and E. P. Chassignet, 2011: Seasonal variation of eddy shedding from the Kuroshio intrusion in the Luzon Strait. *J. Oceanogr.*, **67**, 601–611, doi:10.1007/s10872-011-0060-1.
- , Q. Liu, and W. Liu, 2005: Primary study of the mechanism of eddy shedding from the Kuroshio bend in Luzon Strait. *J. Oceanogr.*, **61**, 1017–1027, doi:10.1007/s10872-006-0018-x.
- Li, L., and Y. Wu, 1989: A Kuroshio Loop Current in the South China Sea? On circulation of the northeastern South China Sea (in Chinese with English abstract). *J. Oceanogr. Taiwan*, **8**, 89–95.
- , W. D. Nowlin, and J. Su, 1998: Anticyclonic rings from the Kuroshio in the South China Sea. *Deep-Sea Res. I*, **45**, 1469–1482, doi:10.1016/S0967-0637(98)00026-0.
- Metzger, E. J., and H. E. Hurlburt, 2001: The nondeterministic nature of Kuroshio penetration and eddy shedding in the South China Sea. *J. Phys. Oceanogr.*, **31**, 1712–1732, doi:10.1175/1520-0485(2001)031<1712:TNNOKP>2.0.CO;2.
- Nan, F., H. Xue, F. Chai, L. Shi, M. Shi, and P. Guo, 2011a: Identification of different types of Kuroshio intrusion into the South China Sea. *Ocean Dyn.*, **61**, 1291–1304, doi:10.1007/s10236-011-0426-3.
- , —, P. Xiu, F. Chai, M. Shi, and P. Guo, 2011b: Oceanic eddy formation and propagation southwest of Taiwan. *J. Geophys. Res.*, **116**, C12045, doi:10.1029/2011JC007386.
- Oey, L.-Y., 2008: Loop Current and deep eddies. *J. Phys. Oceanogr.*, **38**, 1426–1449, doi:10.1175/2007JPO3818.1.
- , T. Ezer, and H. J. Lee, 2005: Loop Current, rings, and related circulation in the Gulf of Mexico: A review of numerical models and future challenges. *Circulation in the Gulf of Mexico: Observations and Models, Geophys. Monogr.*, Vol. 161, Amer. Geophys. Union, 31–56.
- Park, J.-H., and D. Farmer, 2013: Effects of Kuroshio intrusions on nonlinear internal waves in the South China Sea during winter. *J. Geophys. Res. Oceans*, **118**, 7081–7094, doi:10.1002/2013JC008983.
- Pedlosky, J., 1987: *Geophysical Fluid Dynamics*. 2nd ed. Springer-Verlag, 710 pp.
- Qiu, B., and S. Chen, 2004: Seasonal modulation in the eddy field of the South Pacific Ocean. *J. Phys. Oceanogr.*, **34**, 1515–1527, doi:10.1175/1520-0485(2004)034<1515:SMITEF>2.0.CO;2.
- , —, P. Klein, C. Ubelmann, L.-L. Fu, and H. Sasaki, 2016: Reconstructability of three-dimensional upper-ocean circulation from SWOT sea surface height measurements. *J. Phys. Oceanogr.*, **46**, 947–963, doi:10.1175/JPO-D-15-0188.1.
- Qu, T., 2000: Upper-layer circulation in the South China Sea. *J. Phys. Oceanogr.*, **30**, 1450–1460, doi:10.1175/1520-0485(2000)030<1450:ULCITS>2.0.CO;2.
- , H. Mitsudera, and T. Yamagata, 2000: Intrusion of the North Pacific waters into the South China Sea. *J. Geophys. Res.*, **105**, 6415–6424, doi:10.1029/1999JC900323.
- Rio, M.-H., P. Schaeffer, G. Moreaux, J.-M. Lemoine, and E. Bronner, 2009: A new mean dynamic topography computed over the global ocean from GRACE data, altimetry and in situ measurements. CLS/CNES, accessed 10 June 2016. [Available online at http://www.aviso.oceanobs.com/fileadmin/documents/data/products/auxiliary/MDT_Cnes-CLS09_poster_Oceanobs09.pdf.]
- , S. Mulet, and N. Picot, 2013: New global mean dynamic topography from a GOCE geoid model, altimeter measurements and oceanographic in situ data. *Proc. ESA Living Planet Symp.*, Edinburgh, Scotland, ESA. [Available online at http://www.aviso.altimetry.fr/fileadmin/documents/OSTST/2013/oral/mulet_MDT_CNES_CLS13.pdf.]
- Schmitz, W. J., Jr., 2005: Cyclones and westward propagation in the shedding of anticyclonic rings from the Loop Current. *Circulation in the Gulf of Mexico: Observations and Models, Geophys. Monogr.*, Vol. 161, Amer. Geophys. Union, 241–261.
- Sheremet, V. A., 2001: Hysteresis of a western boundary current leaping across a gap. *J. Phys. Oceanogr.*, **31**, 1247–1259, doi:10.1175/1520-0485(2001)031<1247:HOAWBC>2.0.CO;2.
- Su, J. L., 2004: Overview of the South China Sea circulation and its influence on the coastal physical oceanography near the Pearl River estuary. *Cont. Shelf Res.*, **24**, 1745–1760, doi:10.1016/j.csr.2004.06.005.
- Sun, Z., Z. Zhang, W. Zhao, and J. Tian, 2016: Interannual modulation of eddy kinetic energy in the northeastern South China Sea. *J. Geophys. Res. Oceans*, **121**, 3190–3201, doi:10.1002/2015JC011497.
- Tian, J., Q. Yang, and W. Zhao, 2009: Enhanced diapycnal mixing in the South China Sea. *J. Phys. Oceanogr.*, **39**, 3191–3203, doi:10.1175/2009JPO3899.1.
- Volkov, D. L., G. Larnicol, and J. Dorandeu, 2007: Improving the quality of satellite altimetry data over continental shelves. *J. Geophys. Res.*, **112**, C06020, doi:10.1029/2006JC003765.
- Wang, D., H. Z. Xu, J. Lin, and J. Y. Hu, 2008: Anticyclonic eddies in the northeastern South China Sea during winter 2003/2004. *J. Oceanogr.*, **64**, 925–935, doi:10.1007/s10872-008-0076-3.
- Wang, G., J. Su, and P. Chu, 2003: Mesoscale eddies in the South China Sea observed with altimeter data. *Geophys. Res. Lett.*, **30**, 2121, doi:10.1029/2003GL018532.
- , D. Chen, and J. Su, 2008: Winter eddy genesis in the eastern South China Sea due to orographic wind jets. *J. Phys. Oceanogr.*, **38**, 726–732, doi:10.1175/2007JPO3868.1.
- , S.-P. Xie, T. Qu, and R. X. Huang, 2011: Deep South China Sea circulation. *Geophys. Res. Lett.*, **38**, L05601, doi:10.1029/2010GL046626.
- Wu, C.-R., and Y.-C. Hsin, 2012: The forcing mechanism leading to the Kuroshio intrusion into the South China Sea. *J. Geophys. Res.*, **117**, C07015, doi:10.1029/2012JC007968.
- Xie, J., Y. He, Z. Chen, J. Xu, and S. Cai, 2015: Simulations of internal solitary wave interactions with mesoscale eddies in the northeastern South China Sea. *J. Phys. Oceanogr.*, **45**, 2959–2978, doi:10.1175/JPO-D-15-0029.1.
- Xiu, P., F. Chai, L. Shi, H. Xue, and Y. Chao, 2010: A census of eddy activities in the South China Sea during 1993–2007. *J. Geophys. Res.*, **115**, C03012, doi:10.1029/2009JC005657.
- Xu, F.-H., and L.-Y. Oey, 2014: State analysis using the local ensemble transform Kalman filter (LETKF) and the three-layer circulation structure of the Luzon Strait and the South China Sea. *Ocean Dyn.*, **64**, 905–923, doi:10.1007/s10236-014-0720-y.

- Yang, H., and Q. Liu, 2003: Forced Rossby wave in the northern South China Sea. *Deep-Sea Res. I*, **50**, 917–926, doi:[10.1016/S0967-0637\(03\)00074-8](https://doi.org/10.1016/S0967-0637(03)00074-8).
- Yang, Q., W. Zhao, X. Liang, and J. Tian, 2016: Three-dimensional distribution of turbulent mixing in the South China Sea. *J. Phys. Oceanogr.*, **46**, 769–788, doi:[10.1175/JPO-D-14-0220.1](https://doi.org/10.1175/JPO-D-14-0220.1).
- Yuan, D., and Z. Wang, 2011: Hysteresis and dynamics of a western boundary current flowing by a gap forced by impingement of mesoscale eddies. *J. Phys. Oceanogr.*, **41**, 878–888, doi:[10.1175/2010JPO4489.1](https://doi.org/10.1175/2010JPO4489.1).
- , W. Han, and D. Hu, 2006: Surface Kuroshio path in the Luzon Strait area derived from satellite remote sensing data. *J. Geophys. Res.*, **111**, C11007, doi:[10.1029/2005JC003412](https://doi.org/10.1029/2005JC003412).
- , —, and —, 2007: Anti-cyclonic eddies northwest of Luzon in summer–fall observed by satellite altimeters. *Geophys. Res. Lett.*, **34**, L13610, doi:[10.1029/2007GL029401](https://doi.org/10.1029/2007GL029401).
- Zhang, Z., W. Zhao, J. Tian, and X. Liang, 2013: A mesoscale eddy pair southwest of Taiwan and its influence on deep circulation. *J. Geophys. Res. Oceans*, **118**, 6479–6494, doi:[10.1002/2013JC008994](https://doi.org/10.1002/2013JC008994).
- , —, —, Q. Yang, and T. Qu, 2015: Spatial structure and temporal variability of the zonal flow in the Luzon Strait. *J. Geophys. Res. Oceans*, **120**, 759–776, doi:[10.1002/2014JC010308](https://doi.org/10.1002/2014JC010308).
- , J. Tian, B. Qiu, W. Zhao, P. Chang, D. Wu, and X. Wan, 2016: Observed 3D structure, generation, and dissipation of oceanic mesoscale eddies in the South China Sea. *Sci. Rep.*, **6**, 24 349, doi:[10.1038/srep24349](https://doi.org/10.1038/srep24349).
- Zheng, Q., C. Tai, J. Hu, H. Lin, R. Zhang, F. Su, and X. Yang, 2011: Satellite altimeter observations of nonlinear Rossby eddy–Kuroshio interaction at the Luzon Strait. *J. Oceanogr.*, **67**, 365–376, doi:[10.1007/s10872-011-0035-2](https://doi.org/10.1007/s10872-011-0035-2).